Preprint Title Uniform Fe_3O_4/Gd_2O_3-DHCA nanocubes for dual-mode MR imaging

Authors Miao Qin, Yueyou Peng, Mengjie Xu, Hui Yan, Yizhu Cheng, Xiumei Zhang, Di Huang, Weiyi Chen and Yanfeng Meng

Publication Date 15 Apr 2020

Article Type Full Research Paper

ORCID® iDs Di Huang - https://orcid.org/0000-0001-8123-9766; Yanfeng Meng - https://orcid.org/0000-0002-4992-1631

Uniform Fe_3O_4/Gd_2O_3-DHCA nanocubes for dual-mode MR imaging

Miao Qin[1,2,3], Yueyou Peng[2], Mengjie Xu[1,3], Hui Yan[2], Yizhu Cheng[1,3], Xiumei Zhang [1,3], Di Huang*[,1,3], Weiyi Chen[1,3] and Yanfeng Meng*[,2]

Address:

[1] Research Center for Nano-biomaterials & Regenerative Medicine, Department of Biomedical Engineering, College of Biomedical Engineering, Taiyuan University of Technology, Taiyuan, Shanxi 030024, China

[2] Department of MRI, Taiyuan Central Hospital of Shanxi Medical University, Taiyuan, Shanxi 030009, China and

[3] Institute of Biomedical Engineering, Shanxi Key Labratory of Materials Strength & Structrual Impact, Taiyuan University of Technology, Taiyuan, Shanxi 030024, China

Email: yanfeng.m@163.com (Yanfeng Meng), huangjw2067@163.com (Di Huang)

* Corresponding author

Abstract

Multimodal imaging technology were extensively studied over past few years, because they offered complementary diagnosis information, which can increase the accuracy of diagnosis. The synthesis of contrast agents via simplified methods are desired for the development of multimodal imaging. Herein, uniformly distributed Fe_3O_4/Gd_2O_3 nanocubes for T_1-T_2 dual-mode contrast agents were rationally designed and successfully fabricated by our group. In this system, the Fe_3O_4/Gd_2O_3 nanocubes were coated with nontoxic 3,4-dihydroxyhydrocinnamic acid (DHCA) for better hydrophilia

and biocompatibility. The results show that Ferrum (Fe) and Gadolinium (Gd) elements are homo-dispersity in the Fe_3O_4/Gd_2O_3-DHCA (FGDA) nanocubes. Relaxivity study at 3.0 T scanner demonstrates that the r_1 value and r_2 value of FGDA nanocubes reach up to 67.57 ± 6.2 $mM^{-1}s^{-1}$ and 24.2 ± 1.46 $mM^{-1}s^{-1}$. The images of T_1-weighted and T_2-weighted imaging in vivo demonstrate that FGDA nanocubes possess the ability of magnetic resonance (MR) imaging enhancement as dual-mode contrast agent. The above illustrated experimental results indicate that FGDA nanocubes can be applied in clinical diagnosis in future.

Keywords

Fe_3O_4/Gd_2O_3-DHCA nanocubes, dual-mode imaging, Magnetic Resonance Imaging.

Introduction

Magnetic Resonance (MR) imaging has been broadly used in clinical practice for diagnosing disease because of its excellent capability of differentiation of soft tissue, high space resolution, and non-invasive property [1-5]. However, with the increase of disease complexity and the low sensitivity of MR imaging, the diagnosis of diseases has become more and more challenging. Therefore, many researchers have committed to develop contrast agents [6-9]. MR imaging contrast agents can interact with surrounding hydrogen proton to shorten relaxation time and generate signal changes [10]. Generally, contrast agents can be divided into two kinds according to the effect of MR imaging, one is T_1 contrast agents, which shorten longitudinal relaxation time and generate bright signals [11-15], the other is T_2 contrast agents, which shorten transverse relaxation time and generate dark signals [16-17]. The advantage of T_1 contrast agents is that they can generate bright signals, such as Gd-

DTPA, which is broadly used for diagnostic imaging. Nevertheless, the renal toxicity of Gd-based contrast agents should not be ignored [18-19]. T_2 contrast agents have lower toxicity compared to T_1 contrast agents, such as Fe_3O_4 nanoparticle, but the exaggerated artifacts caused by contrast agents disturb the anatomical structure and then affect accuracy of diagnosis. Recent years, most of researchers pay more attention to develop multi-modal contrast agents. T_1-T_2 dual modal MR imaging contrast agents, which could effectively exploit their respective advantages and reduce the adverse impacts [20-21]. Moreover, it also offers complementary diagnostic information, which could improve the sensitivity and reliability for detecting lesions. Fe_3O_4 nanoparticles have been extensively investigated as MRI contrast agents due to their good biocompatibility. Therefore, most of studies of T_1-T_2 dual modal contrast agents are based on Fe_3O_4 nanoparticles in recent years [22].

The present studies demonstrate that uniformly distributed Gd-embedded Fe_3O_4 nanoparticles possess an excellent MR imaging enhancement effect as T_1-T_2 dual modal contrast agent [23]. Moreover, some studies have suggested that nanocubes have a better MR imaging effect compared with nanoparticles. The reason is that cubic shape could induce irreversible dephasing in routine T_2 sequences and a better T_1 MR imaging [24-26]. Inspired by these illustrated studies, we report the fabrication of uniformly distributed cubic shape Fe_3O_4/Gd_2O_3, expecting to obtain a novel nanocubes with better MR imaging enhancement effect. In addition, in present work, the novel nanocubes were coated with 3,4-Dihydroxyhydrocinnamic (DHCA) which has higher exchange efficiency and a lower toxicity compared to frequently used modifications, which could make new nanocubes possess a better water-solubility for more stability in vivo applications [27-28].

Results and Discussion

Synthesis and characterization of FGDA

The schematic illustration of the fabrication of FGDA nanocubes presented in Scheme 1. The oleate metal mixtures as precursors were used to produce Fe_3O_4/Gd_2O_3-Oleic Acid (FGOA) nanocubes by thermal decomposition. In the procedure, reaction temperature and time both play important roles in the size of nanocubes. The FGOA were obtained by refluxing at 310^oC for 30 min. From TEM pictures (Fig 1a, d), it can be seen that the size of cubic FGOA nanocubes are 7.44 ± 0.10 nm and they possess good monodispersity. After the treatment of ligand-exchange, the nanocubes still present good monodispersity, and the size of FGDA nanocubes (about 6.33 ± 0.09 nm), which looks a bit decrease compared to FGOA nanocubes (Fig 1b, e). It may be caused by the change in the surface of nanocubes when FGOA nanocubes were converted to FGDA nanocubes. EDS was performed to study the main element contributions and element distributions of the FGDA nanocubes. EDS spectrum shows mainly ferrum, gadolinium and oxygen elements in the nanocubes. No other impurity elements can be detected except carbon element, which contributes from carbon film on copper mesh. EDS mapping indicates that ferrum and gadolinium elements distribute uniformly in the FGDA nanocubes (Fig 1f, g). In addition, the HRTEM (Fig 1c) shows that the interplanar spacing of nanocubes is 0.296±0.02 nm, which corresponds to (220) crystal plane in Fe_3O_4 [29].

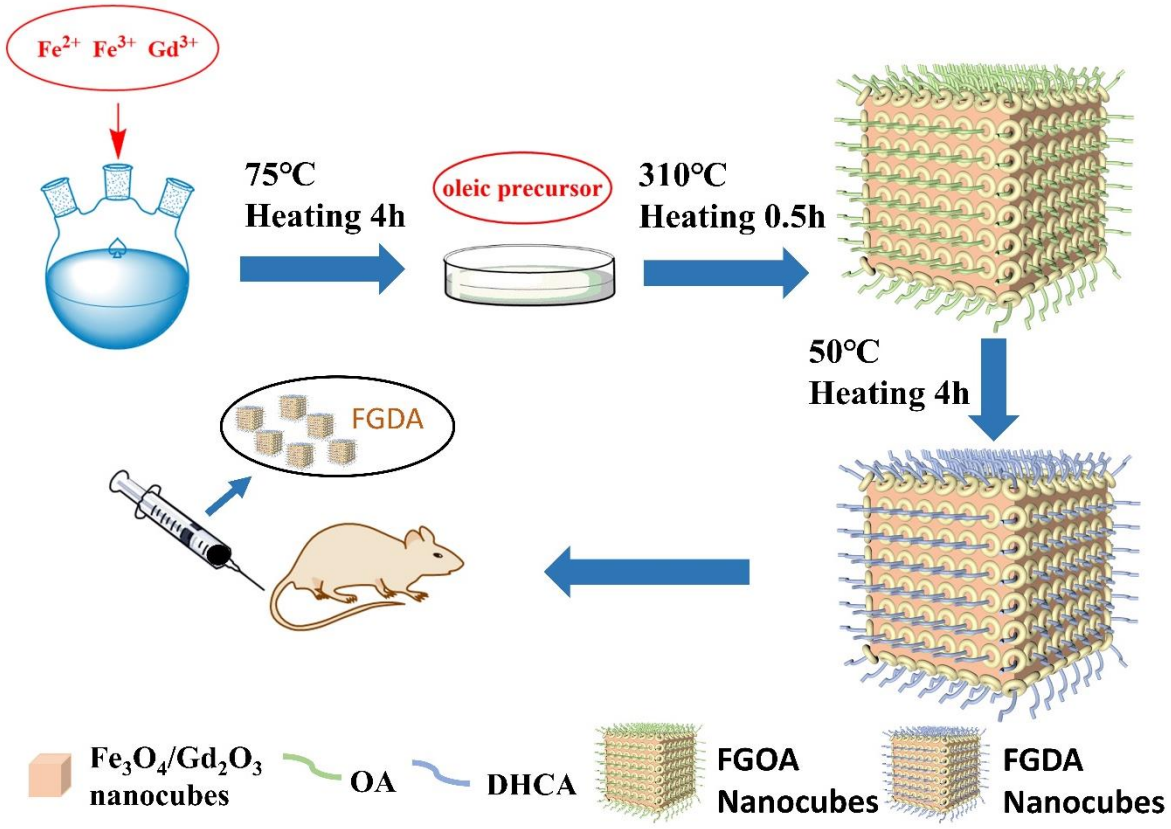

Scheme 1: Schematic illustration of the fabrication of FGDA nanocubes**.**

In order to further confirm the components of FGDA nanocubes, XRD analysis was carried out. As shown in Fig 1h, the major diffraction peaks of Fe_3O_4 at (220), (422), (511), (440) and Gd_2O_3 at (400), (332), (533), (541) are consistent with the diffraction peaks of pure Fe_3O_4 and Gd_2O_3 [23, 30]. The results confirm the nanocubes belong to Fe_3O_4/Gd_2O_3 composites. According to the results, the Fe_3O_4 and Gd_2O_3 crystals uniformly distribute within FGDA nanocubes.

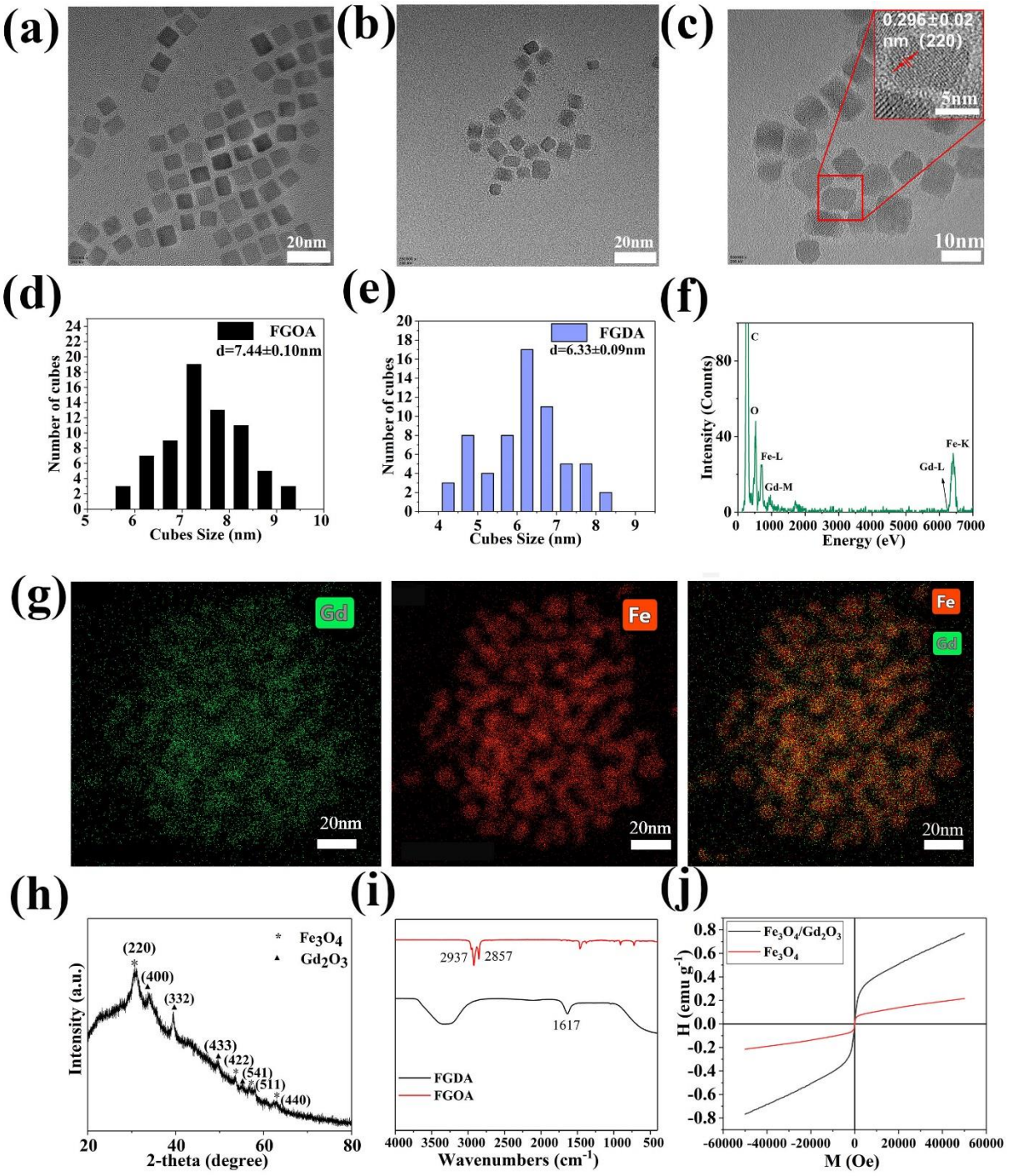

Figure 1: TEM and HRTEM images of (a) FGOA nanocubes, (b, c) FGDA nanocubes; size distribution of (d) FGOA nanocubes and (e) FGDA nanocubes; EDS spectrum of (f) FGDA nanocubes and EDS mapping of (g) Gd, Fe and merged in nanocubes, (h) XRD pattern of FGDA nanocubes, (i) FT-IR spectra of FGOA nanocubes (red line) and FGDA nanocubes (black line), (j) Field-dependent magnetization curves (M-H) of Fe_3O_4/Gd_2O_3 (black line) and Fe_3O_4 (red line) at 300 K.

The FGOA nanocubes exhibit hydrophobic property because of alkyl groups, which limits its application as contrast agent for in vivo use. Therefore, oleic acid on surface of FGOA was considered to be exchanged by DHCA to achieve hydrophilic surface using ligand-exchange method. FT-IR was conducted to verify the surface modifier of the nanocubes with or without DHCA exchange. By comparing the FT-IR spectra of FGOA nanocubes and FGDA nanocubes (Fig 1i), it can be observed that two samples display totally different characteristic absorption peaks. The characteristic absorption peaks of FGOA nanocubes at 2937cm^{-1} and 2857cm^{-1} correspond to the stretching vibration of $–CH_3$ and $–CH_2$, which indicates oleic acid indeed forms on FGOA nanocubes. The characteristic absorption peak of FGDA nanocubes at 1617cm^{-1} corresponds to the stretching vibration of benzene ring skeleton, which indicates that DHCA successfully modifies FGDA nanocubes.

As shown in Fig 1j, the field-dependent magnetization (M-H) curves were conducted at 300 K to estimate the magnetic properties of FGDA nanocubes. Fe_3O_4 nanocubes served as control. It shows that Fe_3O_4 nanocubes and FGDA nanocubes are both superparamagnetic. The saturation magnetization of Fe_3O_4 nanocubes and FGDA nanocubes were 0.2132 emu g^{-1} and 0.7612 emu g^{-1}, respectively. The latter exhibits much higher saturation magnetization than the former, which is probably due to the change of compound structure induced by the addition of gadolinium. The values of saturation magnetization are both low, which may be caused by the small size of nanocubes [31-32].

Relaxation rate measurement

To estimate the MR imaging contrast enhancement of FGDA nanocubes as T_1-T_2 dual-mode contrast agent, MR imaging of FGDA nanocubes sample at different concentrations were conducted to measure r_1 and r_2. Fe_3O_4 nanocubes and Gd_2O_3

nanoparticles were scanned as control. Figure 2 a, and c, show that the MR enhancement of FGDA is better than that of Gd_2O_3 nanoparticles and Fe_3O_4 nanocubes. To investigate the ability of FGDA nanocubes accurately, the r_1 value and r_2 value were calculated to be 67.57 ± 6.2 $mM^{-1}s^{-1}$ and 24.2 ± 1.46 $mM^{-1}s^{-1}$, respectively. Both values present much higher than their control groups. Furthermore , the r_1 value are also higher than the former study [20], it may be caused by the special structure. The investigation confirms that the MR imaging enhancement of FGDA nanocubes containing Fe_3O_4 and Gd_2O_3 is significantly improved compared to pure Gd_2O_3 nanoparticles (r_1 = 11.75 ± 0.62 $mM^{-1}s^{-1}$) and pure Fe_3O_4 nanocubes (r_2 = 2.36 ± 0.59 $mM^{-1}s^{-1}$). It demonstrates that the FGDA nanocubes can be applied in MR imaging as sensitive T_1-T_2 dual modal contrast agent.

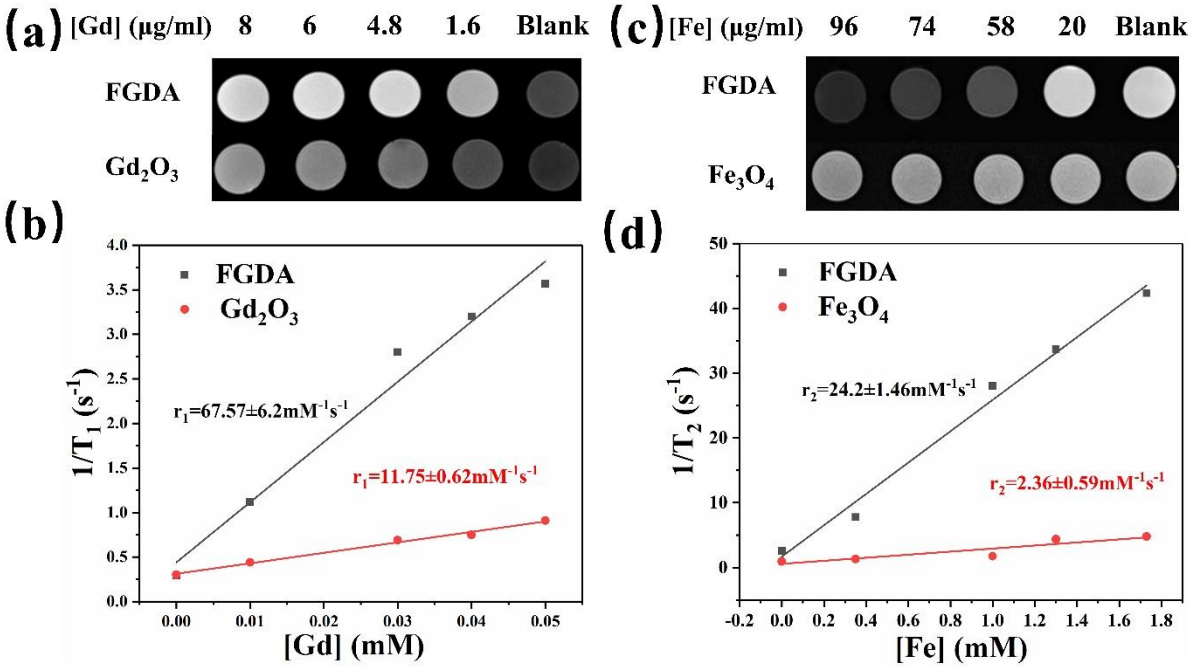

Figure 2: T_1-weigted MR imaging of (a) FGDA nanocubes (top), Gd_2O_3 nanoparticles (bottom) and longitudinal relaxation rate r_1 of (b) FGDA nanocubes (black line) and Gd_2O_3 nanoparticles (red line). T_2-weigted MR imaging of (a) FGDA nanocubes (top), Fe_3O_4 nanocubes (bottom) and transverse relaxation rate r_2 of (b) FGDA nanocubes (black line) and Fe_3O_4 nanocubes (red line).

Biocompatibility

The toxicity of FGDA nanocubes to cells plays an important role in its application [33]. The CCK-8 assay was conducted to detect the viability of L929 cells. Figure 3a indicates that the cell viability of all FGDA nanocubes groups at 12 h have no significant difference compared to control group. The reason may be that L929 cells have to adapt to the medium containing FGDA nanocubes at the initial culturing stage. After culturing 24 h and 48 h, the cell viability of FGDA nanocubes with different Ferrum concentrations shows significantly higher than control group ($p < 0.01$), indicating FGDA nanocubes have no negative influence on the cell proliferation.

The lived-dead staining was performed to further confirm the cytotoxicity of FGDA nanocubes. Form Figure 3b, c, it can be observed that the cellular morphology and proliferation of L929 cells stimulated by FGDA nanocubes have no significant differences compared to control group. The above illustrated investigations present that the FGDA have an excellent biocompatibility to L929 cells, which is the foundation of in vivo applications.

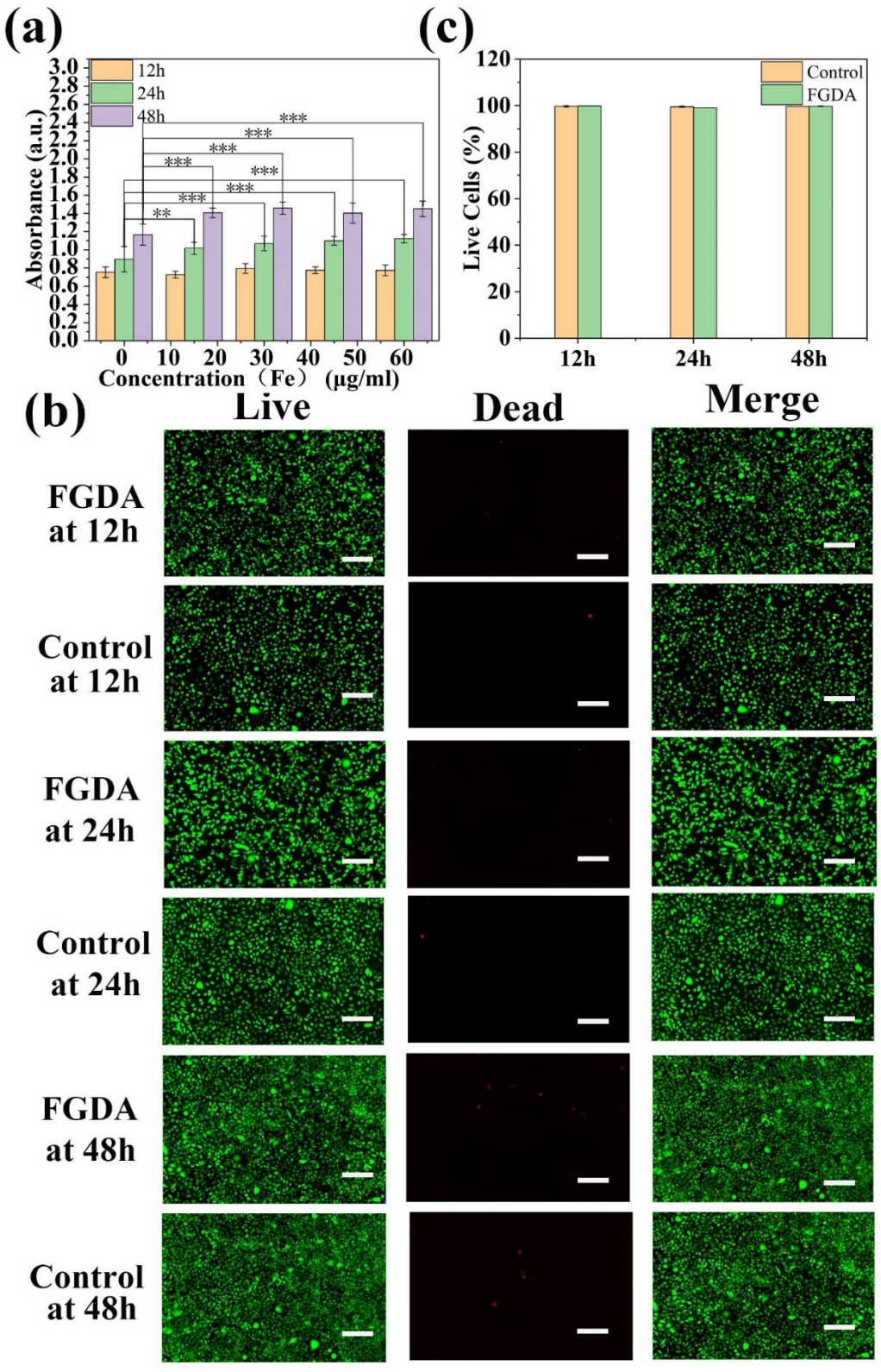

Figure 3: (a) CCK-8 Cell viability of L929 cells incubated with FGDA at different Fe concentrations for 12 h, 24 h and 48 h. (b) Live-Dead staining of control group and FGDA group (Fe concentration: 60μg/ml) after incubation of 12 h, 24 h, 48 h. (c)

Quantitative analysis of live cells as illustrated in (b). Scale bar :100 μm

In vivo MR imaging

To explore MR imaging effect of FGDA nanocubes in vivo, T_1-weighted imaging (T_1WI) and T_2-weighted imaging (T_2WI) of SD rats were accomplished. After intravenous injection of FGDA nanocubes at a dose of 0.8 mg Fe/kg, FGDA nanocubes spread throughout the body along the blood flows. The region of interest we chose was lumber muscle. As shown in Figure 4a~b, T_1WI is significantly enhanced after injection of FGDA nanocubes compared to the pre-injection images. The signal at 30 min (△SNR=5.94%) and 60 min (△SNR=4.18%) post-injection of FGDA nanocubes have attenuated compared with the signal at 10 min post-injection of FGDA nanocubes (△SNR=10.9%). It indicates that T_1 effect of FGDA nanocubes show short-acting in muscle of SD rats. From the bottom images of Figure 4a~c, the signals after injection of FGDA nanocubes at 10 min (△SNR=21.21%), 30 min (△SNR=24.08%) and 60 min (△SNR=32.34%) present higher than the pre-injection in T_2 MR imaging. Furthermore, the signals continue enhancement within an hour, suggesting that the T_2 effect of FGDA nanocubes exhibit long-acting. Prussian blue staining further confirms the presence of irons in lumber muscles, indicating that the signal changes were induced by FGDA nanocubes (fig 4d). The above results prove that the FGDA nanocubes can be applied to diagnosis as T_1-T_2 dual modal contrast agent.

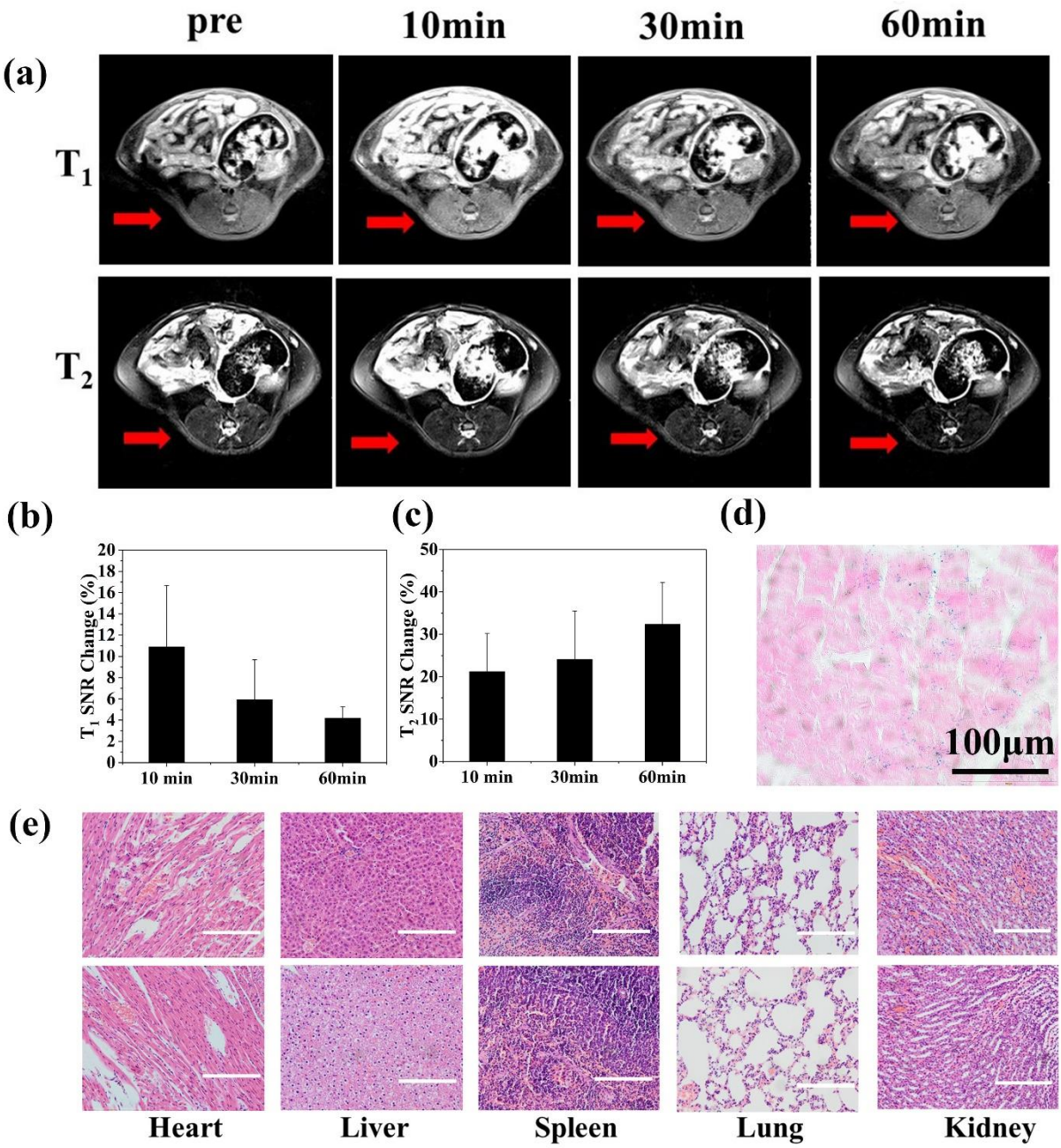

Figure 4: (a) T_1WI and T_2WI in vivo images of SD rats pre- and post- intravenous injection of FGDA nanocubes. (b) T_1 and (c) T_2 SNR change of SD rats pre- and post-intravenous injection of FGDA nanocubes, (d) Prussian blue staining image of lumber muscle on rats intravenously injected FGDA nanocubes, (e) H&E staining of heart, liver, spleen, lung and kidney. Top images: Control group, bottom images: mouse with injection of FGDA nanocubes after 2 weeks. Scale Bar: 200 μm

Tissue staining

Organs of the rats after intravenous injection of FGDA nanocubes at a dose of 2 mg Fe/kg were harvested and fixed. The slices were stained by H&E stain agent to evaluate the toxicity of FGDA nanocubes. It is key point to determine whether FGDA nanocubes are safe for in vivo application. Figure 4e demonstrates that the FGDA nanocubes have no apparent side effects in major organs compared with control group, demonstrating that the FGDA nanocubes were safe.

Conclusion

Uniformly distributed FGDA nanocubes were synthesized by thermal decomposition method. The high r_1 value and r_2 value of FGDA nanocubes represent high quality of MRI enhancement. The cytotoxicity assay, live-dead staining investigation and histological staining study all demonstrate that the FGDA nanocubes possess excellent biocompatibility to cells and animals. The in vivo T_1WI and T_2WI images present the FGDA nanocubes have the excellent capability of enhancement effect as T_1-T_2 dual modal contrast agent in MR imaging. In conclusion, the results show FGDA nanocubes could be served as a potential molecular MRI indicator for both research and clinical diagnosis in future. In addition, a number of special modifications based on FGDA nanocubes will offer new strategies for the future study and clinical practice.

Experimental

Materials

Oleic acid ($C_{18}H_{34}O_2$, OA) and ferric trichloride ($FeCl_3$) were purchased from Tianjin Beichenfangzheng Chemical Reagent Factory. Hexane (C_6H_{14}), ethanol absolute (C_2H_6O), sodium hydroxide (NaOH) and tetrahydrofuran (C_4H_8O, THF) were

purchased from Tianjin Kaitong Chemical Reagent Co, Ltd. Oleylamine ($C_{18}H_{37}N$), 1-Octadecene($C_{18}H_{36}$), sodium oleate ($C_{18}H_{33}NaO_2$), 3,4-dihydroxyhydrocinnamic acid ($C_9H_{10}O_4$, DHCA) and Gadolinium acetate hexahydrate ($C_6H_{11}GdO_7$) were purchased from Rhawn technology Co, Ltd. Ultrapure water was purified by Ulupure (UPR-II, China). All the reagents used in the experiments were of analytical grade and used as received without further purification.

Synthesis of metal oleic precursor

The synthesis methods were described in previous study [34]. 10 mmol Sodium oleate was dissolved in 60 ml ultrapure water and 20 ml ethanol, 5.0 mmol ferric trichloride, 1.0 mmol gadolinium chloride hexahydrate were dissolved in 20 ml ultrapure water in a beaker. Then, the mixture was added to a 250 ml three-necked flask drop by drop. The reaction mixture was heated and refluxed at 75^{o}C for 4 h. The reaction was cooled to room temperature and added 20 ml hexane after accomplished. Then the mixture was transferred to a separating funnel, the organic phase in top was collected in a beaker and the aqueous phase in bottom was discarded. The collected organic phase was washed with water in a separating funnel. The obtained metal oleate complex was dried at 55^{o}C for 24 h to form a ceraceous product. The ferric oleate was synthesized in the similar way.

Synthesis of Fe_3O_4/Gd_2O_3-OA (FGOA) nanocubes

The uniformly distributed FGOA nanocubes were synthesized by one-step thermal decomposition. 1.12 g metal oleate precursor, 0.17 ml oleic acid and 15 ml 1-octadecene were added in a 250 ml three-necked flask. The reaction system was heated up to 200^{o}C and kept the temperature for 30 min and then heated up to 310^{o}C at a rate of 4^{o}C/min and kept refluxing for 30 min. All procedures mentioned above were under nitrogen atmosphere. When the reaction mixture was cooled down to room temperature, 80 ml ethanol was added into the mixture to precipitate the nanocubes.

And the nanocubes were collected by centrifuging at 8000 rotate per min (rpm) for 5 min. Then the obtained hydrophobic nanocubes were washed several times using ethanol and hexane. Finally, the obtained product, FGOA nanocubes, was resuspended in 3 ml hexane.

Synthesis of Fe_3O_4-OA nanocubes

0.92 g Ferric oleate, 0.17 ml oleic acid and 15 ml 1-octadecene were added to a 250 ml three-necked flask. The reaction system was heated up to 200^oC for 30 min and then heated up to 310^oC at a rate of 4^oC/min and kept refluxing for 30 min. The procedures were kept under nitrogen atmosphere. When the reaction mixture was cooled down to room temperature, it should be added 80 ml ethanol to precipitate the nanocubes. And the nanocubes were collected by centrifuging at 8000 rpm for 5 min. Then the obtained hydrophobic nanocubes was washed several times using ethanol and hexane. Finally, the obtained product, Fe_3O_4-OA nanocubes, was resuspended in 3ml hexane.

Synthesis of Gd_2O_3-OA nanoparticles

0.334 g Gadolinium acetate hexahydrate, 4 ml OA, 6 ml oleylamine and 10 ml 1-octadecene were added to a 250 ml three-necked flask. The reaction mixture was heated up to 100^oC for 1 h under nitrogen atmosphere to remove the low volatile impurities and then heated up to 310^oC at a heating rate of 4^oC/min and kept refluxing for 30 min. When the reaction mixture was cooled down to room temperature, 80 ml ethanol was added to precipitate the nanoparticles. And the product was collected by centrifuging at 5000 rpm for 3 min. Then the obtained product was washed by ethanol and hexane. Finally, the obtained product, Gd_2O_3-OA nanoparticles, was resuspended in 3 ml hexane.

Synthesis of aqueous Fe_3O_4/Gd_2O_3-DHCA (FGDA) nanocubes

Briefly, 200 mg DHCA and 60 ml THF were added to a 250 ml three-necked flask under nitrogen, 100 mg FGOA nanocubes and 20 ml THF were added to a beaker. Then the solution in the beaker was added to a three-necked flask drop by drop under nitrogen atmosphere. The reaction mixture was heated up to 50^{o}C and kept refluxing for 4 h under nitrogen atmosphere. When the obtained mixture was cooled down to room temperature, 5 ml NaOH was added into mixture to form a precipitate and the products were collected by centrifuging at 10000 rpm for 10 min. Finally, the aqueous FGDA nanocubes were redispersed in 3 ml ultrapure water. The aqueous Fe_3O_4-DHCA nanocubes and Gd_2O_3-DHCA nanoparticles were synthesized in the similar methods.

Characterizations

High-resolution transmission electron microscope (HR-TEM, JEM-2010F, Japan) operated at an acceleration voltage of 200 kV was used to investigate the morphology and size of nanocubes. The equipped energy dispersive X-ray spectroscopy (EDS, Oxford, X-Max^{N}, UK) was used to analyze the element distribution of samples.

X-ray diffraction (XRD, UltimalV, Japan; Cu Kα (λ = 1.5406Å)) was employed to detect the crystal structure of nanocubes. The diffraction meter was operated at 40 kV, 30 mA. Scan was performed with 2θ value from 20^{o} to 80^{o} at a rate of 0.05^{o} s^{-1}.

Fourier transform infrared (FT-IR) spectra of samples were recorded in the wavenumber range of 4000-400 cm^{-1} using reflection mode (Bruker Alpha, Germany). The Field-dependent magnetization (M-H) curves were obtained from physical property measurement system (Quantum Design, California, USA) at 300 K. Inductive coupled plasma atomic emission spectroscopy (ICP-AES, iCAP7400, Thermo Scientific, USA) was used to test the concentration of Fe and Gd. In vitro and in vivo MR images were obtained from a 3.0 T MRI scanner (MAGNETOM Skyra, Siemens Healthcare, Erlangen, Germany).

The longitudinal (r_1) and transverse (r_2) relaxation rate of the samples were measured to evaluate the properties of the dual-mode contrast agents. The Fe_3O_4-DHCA at different concentrations (0, 20, 58, 74, 96 μg/ml) and Gd_2O_3-DHCA at different concentrations (0, 1.6, 4.8, 6, 8 μg/ml) were conducted as control groups. The nanoparticles were diluted in normal saline. The relaxation rate was measured on the 3.0 T MR scanner with a 15-channel knee coil using T_1-weighted imaging (TR/TE = 1000/11 ms) and T_2-weighted imaging (TR/TE = 4000/70 ms).

Cytotoxicity assay

L929 cells were seeded in a 96-well plate at density of 1×10^4 cell per well and cultured with 200 μl Dulbecco's Modified Eagle's Medium (DMEM, Gibco, Grand Island, USA) supplemented with 10% fetal bovine serum (FBS, Gibco, USA) and 1% Antibiotic-Antimycotic (Thermo Fisher, USA) and incubated at 37°C with 5% carbon dioxide for 24 h. Then the culture medium was discarded and the cells were treated with 15, 30, 45, 60 μg/ml FGDA nanocubes, respectively. The cytotoxicity was evaluated by CCK-8 at 12 h, 24 h, and 48 h. The absorbance was detected using a microplate reader (Biorad iMark, USA) at the wavelength of 450 nm. Each group included six parallel samples.

To intuitively observe the cytotoxicity of FGDA nanocubes, live-dead staining was operated using Calcein AM (C1430, Thermo Fisher, USA) and Ethidium Homodimer 1 (E1169, Thermo Fisher, USA). Briefly, L929 cells were seeded in a 24-well plate at a density of 3×10^4 cell per well. After 24 h incubation, the medium was exchanged with 1 ml cell medium containing 60 μg/ml FGDA nanocubes. The live-dead staining was performed after incubation of 12 h, 24 h and 48 h. Cells were observed by inverted phase contrast microscope (Nikon, TiS, Japan).

In vivo MR imaging

The animal protocol was complied with the regulation of experimental animal management of Shanxi Medical University. Three Sprague Dawley (SD) rats were employed to test the MR imaging effect in vivo of FGDA nanocubes. Under the 2% isoflurane inhalation, MR imaging were performed on rats. T_1WI and T_2WI were acquired by the turbo spin echo (TSE) sequence with the parameter of TR/TE = 550/14 ms and TR/TE = 2510/101 ms, respectively. After FGDA nanocubes were injected through tail vein at a dose of 0.8mg Fe/kg and MR imaging was performed at 10 min, 30 min, and 60 min post-injection.

Histological staining

Immediately after the MR imaging, the rats were euthanized by intravenous injection of overdosed chloral hydrate and the lumber muscles were harvested and placed in 4% paraformaldehyde. Then Prussian blue staining was performed.

In vivo toxicity evaluation of FGDA nanocubes

FGDA nanocubes were injected intravenously into rats at a dose of 2mg Fe/kg. After 2 weeks, the rats were euthanized by intravenous injection of overdosed chloral hydrate and the heart, liver, spleen, lung, kidney were harvested and placed in 4% paraformaldehyde. Then the H&E staining were performed, SD rats of control were injected with normal saline intravenously.

Data analysis

The data were expressed as the means ± standard deviations. Statistical significance was assessed using the Student's t-test, and the values were considered significant at $P < 0.05$.

Acknowledgements

We want to thank Drs. Fenfen Li, Bensheng Qiu, and Qingchen Dong for their technical help.

Funding

This work has been supported by the National Natural Science Foundation of China (Grant No.: 81671789, 11632013, 11502158, 11802197), and the project of Health Commission of Shanxi Province (Grant No.: 2018109). The support of Shanxi Provincial Key Research and Development Project, China (Grant no: 201803D421060) and the Natural Science Foundation for Young Scientist of Shanxi Province, China (201901D111078) is also acknowledged with gratitude.

References

1. Zhang, T. Y.; Li, F. Y.; Xu, Q. H.; Wang, Q. Y.; Jiang, X. C.; Liang, Z. Y.; Liao, H. W.; Kong, X. L.; Liu, J. A.; Wu, H. H.; Zhang, D. P.; An, C. H.; Dong, L.; Lu, Y.; Cao, H. C.; Kim, D.; Sun, J. H.; Hyeon, T.; Gao, J. Q.; Ling, D. S., *Advanced Functional Materials* **2019,** *29* (24), 13.

2. Sehl, O. C.; Makela, A. V.; Hamilton, A. M.; Foster, P. J., *Tomography* **2019,** *5* (4), 367-376.

3. De, M.; Chou, S. S.; Joshi, H. M.; Dravid, V. P., *Advanced Drug Delivery Reviews* **2011,** *63* (14-15), 1282-1299.

4. Anwaier, G.; Chen, C.; Cao, Y. N.; Qi, R., *Int. J. Nanomed.* **2017,** *12*, 7681-7693.

5. Zhu, K.; Ju, Y. M.; Xu, J. J.; Yang, Z. Y.; Gao, S.; Hou, Y. L., *Accounts Chem. Res.* **2018,** *51* (2), 404-413.

6. Snyder, E. M.; Asik, D.; Abozeid, S. M.; Burgio, A.; Bateman, G.; Turowski, S. G.; Spernyak, J. A.; Morrow, J. R., *Angew. Chem.-Int. Edit.*, 7.

7. Botar, R.; Molnar, E.; Trencsenyi, G.; Kiss, J.; Kalman, F. K.; Tircso, G., *Journal of the American Chemical Society* **2020**.

8. Paranawithana, N. N.; Martins, A. F.; Jordan, V. C.; Zhao, P. Y.; Chirayil, S.; Meloni, G.; Sherry, A. D., *Journal of the American Chemical Society* **2019,** *141* (28), 11009-11018.

9. Wang, H.; Jordan, V. C.; Ramsay, I. A.; Sojoodi, M.; Fuchs, B. C.; Tanabe, K. K.; Caravan, P.; Gale, E. M., *Journal of the American Chemical Society* **2019,** *141* (14), 5916-5925.

10. Tóth, É.; Helm, L.; Merbach, A. E., Relaxivity of MRI Contrast Agents. In *Contrast Agents I: Magnetic Resonance Imaging*, Krause, W., Ed. Springer Berlin Heidelberg: Berlin, Heidelberg, 2002; pp 61-101.

11. Gallo, E.; Diaferia, C.; Gregorio, E. D.; Morelli, G.; Gianolio, E.; Accardo, A., *Pharmaceuticals (Basel, Switzerland)* **2020,** *13* (2).

12. Lux, J.; Sherry, A. D., *Curr. Opin. Chem. Biol.* **2018,** *45*, 121-130.

13. Clough, T. J.; Jiang, L. J.; Wong, K. L.; Long, N. J., *Nat. Commun.* **2019,** *10*, 14.

14. Huang, J.; Wang, L. Y.; Zhong, X. D.; Li, Y. C.; Yang, L. L.; Mao, H., *Journal of Materials Chemistry B* **2014,** *2* (33), 5344-5351.

15. Liu, Z.; Cai, J.; Su, H.; Yang, J.; Sun, W.; Ma, Y.; Liu, S.; Zhang, C., *RSC Advances* **2017,** *7* (50), 31671-31681.

16. Lin, K.; Cao, Y.; Zheng, D.; Li, Q.; Liu, H.; Yu, P.; Li, J.; Xue, Y.; Wu, M., *Journal of materials chemistry. B* **2020**.

17. Wang, Y.; Li, X.; Chen, P.; Dong, Y.; Liang, G.; Yu, Y., *Nanoscale* **2020,** *12* (3), 1886-1893.

18. Wei, H.; Bruns, O. T.; Kaul, M. G.; Hansen, E. C.; Barch, M.; Wisniowska, A.; Chen,

O.; Chen, Y.; Li, N.; Okada, S.; Cordero, J. M.; Heine, M.; Farrar, C. T.; Montana, D. M.; Adam, G.; Ittrich, H.; Jasanoff, A.; Nielsen, P.; Bawendi, M. G., *Proceedings of the National Academy of Sciences of the United States of America* **2017,** *114* (9), 2325-2330.

19. Weng, Q. J.; Hu, X.; Zheng, J. H.; Xia, F.; Wang, N.; Liao, H. W.; Liu, Y.; Kim, D.; Liu, J. A.; Li, F. Y.; He, Q. J.; Yang, B.; Chen, C. Y.; Hyeon, T.; Ling, D. S., *Acs Nano* **2019,** *13* (6), 6801-6812.

20. Li, F. F.; Zhi, D. B.; Luo, Y. F.; Zhang, J. Q.; Nan, X.; Zhang, Y. J.; Zhou, W.; Qiu, B. S.; Wen, L. P.; Liang, G. L., *Nanoscale* **2016,** *8* (25), 12826-12833.

21. Lu, C. C.; Dong, P. L.; Pi, L.; Wang, Z. J.; Yuan, H. X.; Liang, H. Y.; Ma, D. G.; Chai, K. Y., *Langmuir* **2019,** *35* (29), 9474-9482.

22. Zhao, H. Y.; Liu, L.; He, J.; Pan, C. C.; Li, H.; Zhou, Z. Y.; Ding, Y.; Huo, D.; Hu, Y., *Biomaterials* **2015,** *51*, 194-207.

23. Zhou, Z.; Huang, D.; Bao, J.; Chen, Q.; Liu, G.; Chen, Z.; Chen, X.; Gao, J., *Advanced Materials* **2012,** *24* (46), 6223-6228.

24. Zhou, Z. J.; Yang, L. J.; Gao, J. H.; Chen, X. Y., *Advanced Materials* **2019,** *31* (8), 32.

25. Lee, N.; Choi, Y.; Lee, Y.; Park, M.; Moon, W. K.; Choi, S. H.; Hyeon, T., *Nano Letters* **2012,** *12* (6), 3127-3131.

26. Yang, L. J.; Zhou, Z. J.; Liu, H. Y.; Wu, C. Q.; Zhang, H.; Huang, G. M.; Ai, H.; Gao, J. H., *Nanoscale* **2015,** *7* (15), 6843-6850.

27. Liu, Y.; Chen, T.; Wu, C. C.; Qiu, L. P.; Hu, R.; Li, J.; Cansiz, S.; Zhang, L. Q.; Cui, C.; Zhu, G. Z.; You, M. X.; Zhang, T.; Tan, W. H., *Journal of the American Chemical Society* **2014,** *136* (36), 12552-12555.

28. Liu, Y.; Purich, D. L.; Wu, C. C.; Wu, Y.; Chen, T.; Cui, C.; Zhang, L. Q.; Cansiz, S.; Hou, W. J.; Wang, Y. Y.; Yang, S. Y.; Tan, W. H., *Journal of the American Chemical*

Society **2015,** *137* (47), 14952-14958.

29. Park, S. I.; Kwon, B. J.; Park, J. H.; Jung, H.; Yu, K. H., *J. Nanosci. Nanotechnol.* **2011,** *11* (2), 1818-1821.

30. Peng, H. X.; Cui, B.; Li, L. L.; Wang, Y. S., *J. Alloy. Compd.* **2012,** *531*, 30-33.

31. Jun, Y. W.; Huh, Y. M.; Choi, J. S.; Lee, J. H.; Song, H. T.; Kim, S.; Yoon, S.; Kim, K. S.; Shin, J. S.; Suh, J. S.; Cheon, J., *Journal of the American Chemical Society* **2005,** *127* (16), 5732-5733.

32. Lee, J. S.; Cha, J. M.; Yoon, H. Y.; Lee, J. K.; Kim, Y. K., *Sci Rep* **2015,** *5*, 7.

33. Sharifi, S.; Behzadi, S.; Laurent, S.; Laird Forrest, M.; Stroeve, P.; Mahmoudi, M., *Chemical Society Reviews* **2012,** *41* (6), 2323-2343.

34. Park, J.; An, K.; Hwang, Y.; Park, J.-G.; Noh, H.-J.; Kim, J.-Y.; Park, J.-H.; Hwang, N.-M.; Hyeon, T., *Nature materials* **2004,** *3* (12), 891-5.